Theory of optical properties of 6.1 Å III–V superlattices: The role of the interfaces

Rita Magri and Alex Zunger

Theory of optical properties of 6.1 Å III–V superlattices: The role of the interfaces

Rita Magri
Istituto Nazionale per la Fisica della Materia, S^3, and Dipartimento di Fisica Universitá di Modena e Reggio Emilia, Via Campi 213/A, Modena, Italy

Alex Zunger
National Renewable Energy Laboratory, Golden, Colorado 80401

Interfacial interdiffusion in quantum wells and superlattices could alter the interfacial strain, band alignment, and even the atomic symmetry at the interface, thus potentially changing the electronic and optical properties. We consider the InAs/GaSb system describing the interdiffused interfaces via a simple kinetic model of molecular beam epitaxy growth. The predicted atomic positions after interdiffusion are then used in a pseudopotential theory to describe the electronic and optical consequences of interdiffusion. We determine (i) the effects of different interfacial bonding compositions on the electronic and optical properties; (ii) the segregation profiles at the normal and inverted interfaces; and (iii) the effect of structural disorder on band gaps. The application of our method to the InAs/GaSb superlattices allows us to explain numerous observed results and trends. © *2003 American Vacuum Society.* [DOI: 10.1116/1.1589519]

I. INTRODUCTION

Superlattices and quantum wells between InAs and GaSb are interesting for a few reasons:

(i) Unusual band allignment: the conduction-band minimum (CBM) of InAs is below the valence-band maximum (VBM) of GaSb. This type II "broken gap" band alignment provides the ability to tune the effective separation between the lowest confined conduction subband $e1$ and the highest valence subband hh1 in the technologically important 2–10 μm range by varying the thicknesses of the InAs and GaSb layers. This tunability of the band gap has made this system technologically interesting for infrared lasers and detectors.[1] However, the application to such devices requires the use of very thin layers of InAs and GaSb for two reasons. First, only for thin layers does the electron and hole quantum confinement cause the InAs/GaSb system to be a semiconductor. Second, thin InAs and GaSb layers are needed to create sufficient wave-function overlap, so the spatial separation of carriers in type II structures will not cause the hole and electron wave-function overlap to vanish. However, when thin layers are used, any deviation from perfect atomic layer-by-layer growth could greatly affect the electronic properties.

(ii) The InAs/GaSb superlattice has unusually low spatial symmetry due to its no-common-atom nature: since the two binary compounds InAs and GaSb lack a common atomic element, the superlattices InAs/GaSb have a lower C_{2v} point group symmetry than common-atom superlattices such as InAs/GaAs or AlAs/GaAs whose symmetry is D_{2d}. The lower symmetry of InAs/GaSb is manifested by the existence of unequal bonds at the two opposite interfaces. The ensuing low C_{2v} symmetry causes couplings between the wave functions of different bands, including the Brillouin zone center, and this has a number of effects on the electronic structure and the optical properties. First, it leads to the appearance of parity *forbidden* lh1↔$e2$ and hh2↔$e1$ transitions.[2] Second,

it causes energy band anticrossings and subsequent shifts of the transition energies that are easily observed for given superlattice periods.[3] Third, it causes also the $e1$↔hh1 and $e1$↔lh1 transitions to develop an in-plane polarization anisotropy whereby the dipole transitions have unequal strength along the [110] and [−110] in-plane directions.[4] Such effects are unique to C_{2v} superlattices with inequivalent interfaces and are expected to drastically change as the superlattice interfaces are modified. Finally, a new interface inversion asymmetry term appears in the Hamiltonian and gives a contribution to the zero field spin splitting.[5] The effects on the electronic structures listed above and due to the lower C_{2v} symmetry cannot be predicted by the conventional eight band $\mathbf{k} \cdot \mathbf{p}$ model,[6] which does not "see" the correct atomistic C_{2v} or D_{2d} symmetry, confusing it with T_d.

(iii) Interfacial segregation/mixing strongly affects the optical properties. Because of factors (i) and (ii) above, deviations from the ideal abrupt interfacial geometry which are always present due to segregation, diffusion, and exchanges with the molecular/vapor phases, are particularly critical in InAs/GaSb. Recent cross-sectional scanning tunneling microscopy measurements on InAs/InGaSb superlattices have indeed observed Sb penetration into InAs, and As penetration into the first few layers of InGaSb.[7]

Recent optical experiments have highlighted the importance of the interface morphology on the electronic properties of the InAs/GaSb system. Yang *et al.*[8] found a 30–40 meV increase of the band gap of a $(InAs)_{5.5}/(In_{0.28}Ga_{0.72}Sb)_{10}/(InAs)_{5.5}/(AlSb)_{14}$ structure, when the layer thicknesses were kept constant but the growth temperature of the device was increased from 460 to 500 °C. This suggests that interdiffusion changes the band gap. Besides having such large variations in the band gap for nominally identical structures grown by the same grower, there are large variations in band gaps of the same structure grown

by different growers. Vurgaftman and Meyer[9] showed that there are conspicuous differences between the band gaps derived using data from different growers. In some cases they found differences as large as 200 meV in the predicted VBO for the InAs/GaSb system, even for structures nominally quite similar. Experiments have also shown that, besides interfacial disorder effects, even the nature of the interfacial bonds has a conspicuous effect on the band gap energy. Bennett et al.[10] measured the band gaps of InAs/GaSb superlattices grown in such a way so to have or almost pure InSb-like or almost pure GaAs-like interfaces and found a difference of 40 meV for superlattices with a nominal period $n = 8$. In particular, gaps $E_g = 209$ and 216 meV have been measured for two samples with In–Sb-like interfaces, whereas a gap $E_g = 253$ meV was measured for a sample with only GaAs-like interfaces. Clearly, the atomic-level structure at the interface controls the band gap.

We have previously shown[11] that the "standard model" based on continuum-like effective-mass $\mathbf{k} \cdot \mathbf{p}$ approaches is insufficient to describe the electronic structure of such thin superlattices, even if they are assumed to be abrupt. A good theory should take into account the effects on the band structure of segregation and interfacial atomic intermixing to provide accurate values.

In this article, we use a kinetic model of interfacial segregation during molecular beam epitaxy (MBE) growth. We find the atomic positions near the interface after segregation at a given growth temperature and deposition rate. We, then, use these atomic concentration profiles in a pseudopotential calculation of the electronic structure. By comparing optical and electronic properties before and after segregation, we pinpoint the atomistic effects of segregation on optical properties.

II. THEORETICAL METHOD

We solve the single-particle Schrödinger equation:

$$\left[-\frac{\beta}{2} \nabla^2 + \sum_{n\alpha} v_\alpha(r - R_{n\alpha}) \right] \psi_i(r) = \epsilon_i \psi_i(r), \quad (1)$$

where $R_{n\alpha}$ denotes the position of the nth ion of type α (=In, Ga, As, Sb). Thus, the crystal potential is written as a superposition of atomic potentials, v_α, centered around the atomic sites. The potential includes the spin–orbit interaction, thus the wave functions $\psi_i(r)$ are spinors with spin up and spin down components. For the potential v_α we do not use the local density approximation (LDA), since not only it produces the well-known[12] LDA errors in band gaps, but also the all-important effective masses are considerably in error. Instead, we use empirically fitted atomic *screened* pseudopotentials. The full symmetry of the system is determined authomatically by the atomic positions. The term β, which scales the kinetic energy in the Schrödinger equation, has been introduced to represent the quasiparticle nonlocal self-energy effects.[13] In fact, it can be shown that at the lowest order, the leading effects of the nonlocal many body potential

can be represented by scaling the kinetic energy.[14] This kinetic energy scaling is needed to simultaneously fit bulk effective masses and band gaps.

In the traditional implementations of the empirical pseudopotential method the crystal potential is written in terms of few form factors $V(\mathbf{G_i})$ relative to the reciprocal lattice vectors $\mathbf{G_i}$ of the binary bulk solids. On the other hand, applications to nanostructures and alloys, which have much larger unit cells, require the determination of $V(\mathbf{G})$ at many intermediate previously unknown values. We address this point by determining the atomic screened pseudopotential form factors $v_\alpha(\mathbf{q})$ as *continuous* functions of momentum $\mathbf{q}$, for the atomic species α=Ga, Sb, In, As of the quaternary GaSb/InAs system. We fit the parameters entering the expression of the form factors to the experimentally measured electron and hole effective masses,[15] band gaps (target values at 0 K),[15] spin–orbit splittings,[15] hydrostatic deformation potentials of the band gaps,[15] band offsets,[15] and LDA-predicted single band edge deformation potentials[16] of the four *binary* systems. The results of the fit are given elsewhere.[17] This procedure allows us to describe the interface-specific bonds as individual Ga–As and In–Sb bonds whose chemically properties are related to those of the parent bulk compounds.

The traditional form of the empirical pseudopotential approach[18] is strain independent. Not surprisingly the dependence of the valence-band maximum and conduction-band minimum on the hydrostatic deformations was discovered to have often the incorrect sign.[19] To obtain the correct behavior of the band-edge energies under hydrostatic or biaxial strain deformations we have built the response to the strain directly into the screened atomic pseudopotetials v_α, adding an explicit strain dependent term $\delta v_\alpha(\epsilon)$. This term plays a crucial role in describing the variation of the valence-band edge and, separately, the conduction-band edge under arbitrary strains. This allows us to describe the modification of the valence- and conduction-band offsets when the systems are subjected to hydrostatic or biaxial deformation conditions such as in the case of epitaxial growth on a lattice-mismatched substrate. Note that even though the binary GaSb and InAs systems are nearly lattice matched (the lattice mismatch is relatively small, 0.6%), the quaternary systems manifest at the interface also, Ga–As and In–Sb bonds which have a huge mutual lattice mismatch of 14% and are also strongly mismatched (by about 6%–7%) with respect to the Ga–Sb and In–As bonds. We fitted not only the experimental hydrostatic deformation potentials of the band gap, but also the *ab initio* calculated hydrostatic deformation potentials of the valence-band maximum.[16] Our scheme takes into account authomatically the change in the valence- and conduction-band offsets of the system due to changes in the biaxial constraints or local bonding deformations without the need to readjust any parameter.

In the InAs/GaSb system, we need to apply our scheme to different atomic local environments than those present in the fitted pure binary compounds. We address the problem of the transferibility of the screened potentials to different atomic

environment considering only the nearest-neighbor environment. In the quaternary $(AC)(BD)$ systems, the C and D anions can be surrounded by A_nB_{4-n} cations, where $n = 0, 1, 2, 3,$ and 4. Analogously, the A and B cations can be surrounded by C_nD_{4-n} anions. Our EPM has been obtained by fitting the properties of only the pure binary compounds (corresponding to environments $n = 0$ and $n = 4$). To improve the transferibility to other environments, we assume a linear interpolation between these limits as

$$v_A(C_nD_{4-n}) = \frac{n}{4}v_A(AC) + \frac{4-n}{4}v_A(AD),$$

$$v_B(C_nD_{4-n}) = \frac{n}{4}v_B(BC) + \frac{4-n}{4}v_B(BD),$$

$$v_C(A_nB_{4-n}) = \frac{n}{4}v_C(AC) + \frac{4-n}{4}v_C(BC),$$

$$v_D(A_nB_{4-n}) = \frac{n}{4}v_D(AD) + \frac{4-n}{4}v_D(BD). \tag{2}$$

AC, BC, AD, and BD are the four binary compounds, in our case GaSb, GaAs, InSb, and InAs, whose properties have been directly fitted to extract the atomic pseudopotential parameters. This procedure leads to a potential for the InAs monolayers closer to the interface different from the potential of the InAs monolayers in bulk InAs, in agreement with the results of more accurate self-consistent calculations.

An empirical pseudopotential calculation requires: (a) to determine a reliable equilibrium atomic configuration for the system, and (b) to calculate the band structure relative to that given atomic configuration. To determine the atomic positions $R_{n\alpha}$ we minimize the elastic energy corresponding to a given atomic arrangement in the system, via the valence force field approach.[20] For (b) we expand the wave functions $\psi_i(r)$ in a plane-wave basis. The Hamiltonian matrix elements are calculated in this basis with no approximation, then the Hamiltonian matrix is diagonalized via the folded spectrum method.[21]

III. RESULTS

A. Superlattices with abrupt interfaces

Figure 1 shows the electron $E1$ and hole (HH1,LH1,HH2) levels of $(\mathrm{InAs})_n/(\mathrm{GaSb})_n(001)$ superlattices as a function of n. We see that as n is reduced from infinity, the $E1$ level moves up, while HH1, LH1, and HH2 move down, all states becoming more and more confined within the corresponding wells. When $n < 28$ the superlattices acquire a semiconducting gap with the first electron state $E1$ localized in the InAs layer and the first hole state HH1 localized in the GaSb layer. At $n \geq 28$ the energy of the $E1$ level becomes lower than the energy of the hole HH1 state. At $n \approx 28$ the $E1$ level and the HH1 level should cross. However, because of the reduced C_{2v} symmetry of the superlattices, the two levels anticross. The anticrossing gap opens at $k_\parallel = 0$ and its calculated value is $E_A^{\mathrm{HH1},E1} = 11$ meV. We find a strong wave-function mixing
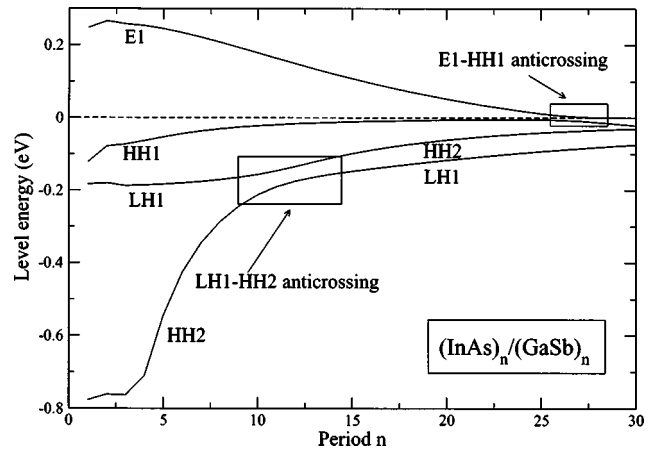

FIG. 1. Level energies of the $E1$, HH1, LH1, and HH2 states of $(\mathrm{InAs})_n/(\mathrm{GaSb})_n$ superlattices as a function of layer thickness n. Dashed line denotes the VBM of bulk GaSb.

at the HH1−$E1$ anticrossing. The superlattice period at which the anticrossing gap occurs is in good agreement with other calculations.[22]

In addition to $E1-$HH1 coupling and anticrossing we also find anticrossing between the hole levels LH1 and HH2 around $n = 13$ (see Fig. 1). For superlattice periods n close to $n = 13$ the wave functions of the two hole states strongly intermix. The calculated anticrossing gap is $E_A^{\mathrm{LH1,HH2}} = 40$ meV. This causes the appearance of new transitions LH1$\leftrightarrow$E2 and HH2$\leftrightarrow$E1 in the spectra that become allowed because of this mixing. These effects are due to the superlattice low spatial symmetry and are not taken into account in the standard envelope function approaches.

At $n > 28$, one expects a metallic state. However, even for superlattices with a InAs layer large enough for the $E1$ level to fall well *below* the HH1 level at $k_\parallel = 0$, a small anticrossing gap is found at some in-plane wave vectors $\mathbf{k}_\parallel^*$. Figure 2 describes the band structure of the $(\mathrm{InAs})_{46}(\mathrm{GaSb})_{14}$ superlattice. On the right side, we show the in-plane dispersion along the [1,1,0] direction ($k_x = k_y$) corresponding to the
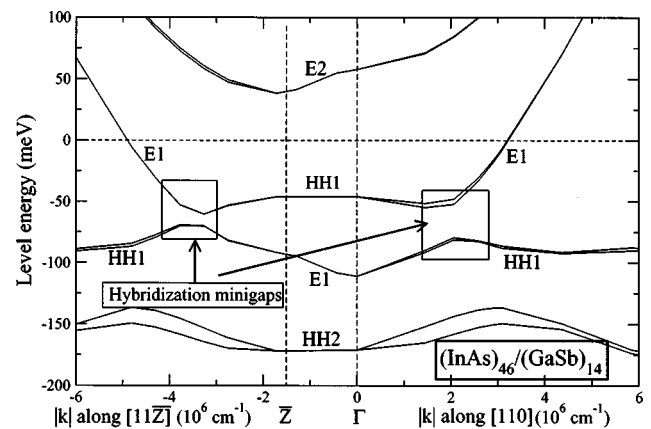

FIG. 2. Dispersion relations for the $(\mathrm{InAs})_{46}/(\mathrm{GaSb})_{14}(001)$ superlattice. Indicated by arrows and encircled by boxes are the hybridation minibands formed by the $E1$ and HH1 anticrossing away from the Brillouin zone center. Dashed line indicates the energy of the GaSb VBM.

$k_z = 0$ plane, while on the left side we show the in-plane $(k_x = k_y)$ dispersion corresponding to $k_z = \bar{Z}$ where $\bar{Z} = \pi/60a$, a being the lattice parameter. In the central part we give the dispersion with k_z from $\bar{\Gamma}$ to $\bar{Z}$, where $\bar{Z}$ is the point at the border of the Brillouin zone along the k_z direction. Thus, we still have a semiconducting superlattice (SL) because of the overlap of the hybridization minigaps formed along different directions of the Brillouin zone.

Moving in the Brillouin zone towards and across the hybridization minigaps, one observes that the wave functions exchange their character: the lower band becomes H_{GaSb}, while the higher becomes E_{InAs}. We see from the calculated dispersion relations shown in Fig. 2 that the minimum hybridization gap occurs for abrupt superlattices at some $\mathbf{k}_\parallel^*$ $\neq 0$ at $k_z = \bar{Z}$, and is about 8 meV wide. In contrast, in the plane $k_z = 0$ the hybridization gap occurs at a slightly larger $\mathbf{k}_\parallel^*$ and has a larger value of 25 meV. Yang et al.[23] detected, using capacitance–voltage measurements on nominally $(InAs)_{46}/(GaSb)_{14}$ superlattices, a small band gap (≈ 4 meV).

B. Dependence of the band gaps on the composition of the interfaces

We have calculated the value of the fundamental band gap of the $(InAs)_8/(GaSb)_8$ superlattices, where we have changed the composition of the interface bonds in an otherwise ideal abrupt structure, by swapping only one interface anion plane from Sb to As or vice versa. In this way, we end up with a $(InAs)_{7.5}/(GaSb)_{8.5}$ superlattice with two In–Sb interfaces and a $(InAs)_{8.5}/(GaSb)_{7.5}$ superlattice with two Ga–As interfaces. The calculated band gaps are $E_g = 229$ meV for the structure with two In–Sb interfaces, $E_g = 279$ meV for the structure with two Ga–As interfaces and $E_g = 238$ meV for the structure with one In–Sb interface and one Ga–As interface. We can compare these values with the experimental results. The measured band gaps are $E_g^{expt} = 209/216$ meV for the structure with two InSb interfaces, and $E_g^{expt} = 253$ meV for the structure with two Ga–As interfaces.[10] The superlattices with a larger number of Ga–As interfacial bonds are correctly predicted to have an higher band gap. Moreover, the calculated value of the difference between the band gaps, 50 meV, compares well with the measured value,[10] 40 meV.

C. Band bowing of ternary alloys

An important test of the capability of our scheme to treat properly disorder effects in the quaternary InAs/GaSb system is the prediction of the band bowings of all the ternary alloys. The ternary random $In_xGa_{1-x}As$, $In_xGa_{1-x}Sb$, $GaAs_{1-x}Sb_x$, and $InAs_{1-x}Sb_x$ alloys are modeled by occupying randomly the sites of a 512 atom cubic supercell for compositions $x = 0.25$, 0.50, and 0.75. For each alloy configuration, the atomic positions were relaxed using the valence force field (VFF) method,[20] while the supercell size is determined by a lattice constant given by the composition average of the lattice constants of the constituent binary
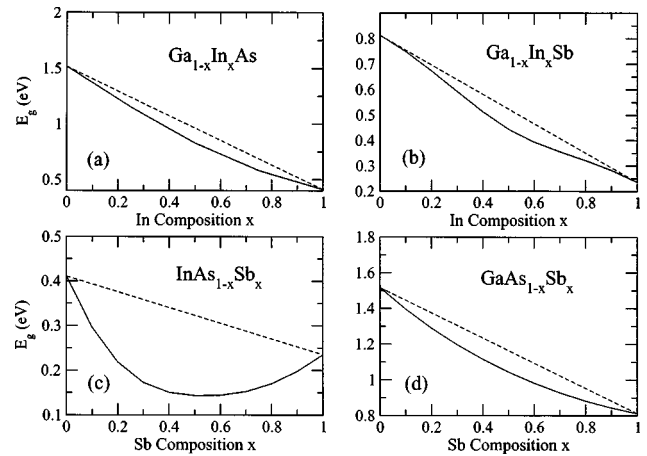

FIG. 3. Calculated band gaps of the ternary (a) $Ga_{1-x}In_xAs$, (b) $Ga_{1-x}In_xSb$, (c) $InAs_{1-x}Sb_x$, and (d) $GaAs_{1-x}Sb_x$ alloys vs composition x. Dashed lines indicate the linear weighted averages.

compounds following the Vegard's law. The calculated optical band bowings are correctly predicted positive, and in the case of the $InAs_{1-x}Sb_x$ ternary alloy, we find the absolute minimum gap around $x = 0.5$ in good agreement with experiment.[15] In Fig. 3 we show the dependence of the band gaps of the ternary alloys versus composition. We obtain the following bowing parameters: for the $In_{0.5}Ga_{0.5}As$ alloy a value $b = 0.54$ [expt. 0.49, 0.61 (Ref. 15)], for the $In_{0.5}Ga_{0.5}Sb$ alloy $b = 0.32$ [expt. 0.42 (Ref. 15)], for the $InAs_{0.5}Sb_{0.5}$ alloy $b = 0.72$ [expt. 0.67,[9] 0.76 (Ref. 15)]. Only for the $GaAs_{0.5}Sb_{0.5}$ alloy the calculated bowing, 0.53, is definitely smaller than the experimental value, 1.0.[15] Perhaps more-detailed calculations of the alloy band gap, taking into account also ordering effects (the $GaAs_{0.5}Sb_{0.5}$ alloy is known, indeed, to present spontaneous ordering in the chalcopyrite structure, which lowers considerably the fundamental gap), need to be performed.

We stress here that the band gaps of the alloys have not been fitted. Differently from other methods[22] where new sets of parameters must be determined for each alloy system and for each alloy composition, here we have obtained the band gaps of all the ternary alloys at all compositions having fitted only the binary compounds.

D. Kinetic model of molecular beam epitaxy growth of the InAs/GaSb superlattices

To generate composition profiles for GaSb/InAs superlattices we have relied on a kinetic model for MBE growth, first introduced by Dehaese et al.,[24] which we have extended to treat simultaneously segregation both of group III and of group V species in the no-common-atom quaternary GaSb/InAs system. The model simulates a layer-by-layer growth starting from a given substrate, and, at each interface, segregation is determined by atomic exchanges between the surface layer and the first subsurface layer, for each sublattice (cation and anion) separately. Layer growth is driven by the impinging atomic fluxes Φ_{In}, Φ_{Ga}, Φ_{sb}, and Φ_{As} (in ML/s). Atomic exchanges require overcoming energetic barriers for

bulk-to-surface ($b \rightarrow s$) and surface-to-bulk ($s \rightarrow b$) atomic swaps. For the cation system we have the barrier $E_{\text{In/Ga}}^{b \rightarrow s}$ for subsurface In to exchange with surface Ga, and $E_{\text{In/Ga}}^{s \rightarrow b}$ for surface In to exchange with subsurface Ga. Similarly, we have $E_{\text{Sb/As}}^{b \rightarrow s}$ and $E_{\text{Sb/As}}^{s \rightarrow b}$ with similar meanings. The segregation driving forces are proportional to

$$\Delta_{\text{In/Ga}} = E_{\text{In/Ga}}^{s \rightarrow b} - E_{\text{In/Ga}}^{b \rightarrow s},$$
$$\Delta_{\text{Sb/As}} = E_{\text{Sb/As}}^{s \rightarrow b} - E_{\text{Sb/As}}^{b \rightarrow s}. \quad (3)$$

Here, $\Delta_{In/Ga} > 0 (<0)$ implies In (Ga) segregation to the surface, whereas $\Delta_{\text{Sb/As}} > 0 (<0)$ implies Sb (As) segregation. The rates of $i = b \rightarrow s$ or $i = s \rightarrow b$ exchange reactions at growth temperature T_g are $P_i = \nu_i \exp[-(E_{\alpha/\beta}^i / k_B T_g)]$, where k_B is the Boltzmann constant and ν_i is the effective hopping frequency for which we use the commonly accepted value of 10^{13} s^{-1} for III–V compounds.[24] Denoting by A and B the two different kinds of atoms in one sublattice (e.g., In and Ga), the rate of change of the concentration $x_A(t)$ of surface A atoms is given by[24]

$$\frac{dx_A^s(t)}{dt} = \Phi_A + P_1 x_A^b(t) \cdot x_B^s(t) - P_2 x_A^s(t) x_B^b(t). \quad (4)$$

Here, $x_A^{s,b}(t)$ and $x_B^{s,b}(t)$ are the time-dependent concentrations of A and B at the surface or bulk, the first term Φ_A is the deposition rate of A atoms onto the surface, the second term is the rate of A atoms arriving from subsurface to the surface after exchanging with surface B atoms, and the last term is the rate of A atoms leaving the surface after exchanging with bulk B atoms. The conservation of A atoms and of the total number of surface atoms at any time t leads to the conditions:

$$x_A^s(t) + x_A^b(t) = x_A^s(t) + x_A^b(t) + \Phi_A t, \quad (5)$$

$$x_A^s(t) + x_B^s(t) = x_A^s(0) + x_B^s(0) + (\Phi_A + \Phi_B)t, \quad (6)$$

and, at any t, we have $x_A^b(t) + x_B^b(t) = 1$. A small fraction x_0 of the segregating Sb specie is incorporated into each InAs layer during the growth because of an unwanted vapor background. This cross incorporation has been taken into account modifying slightly the fluxes Φ_{As} and Φ_{Sb} during the growth of InAs so as to have the incorporation of a small constant Sb fraction $x_0 = 0.015$ into each InAs layer.

We solve numerically Eqs. (4)–(6) for $A =$ Ga, In, As, and Sb. The input to the simulation consists of growth temperature T_g, atomic fluxes Φ_α, $\alpha =$ Ga, In, As, and Sb, and the four exchange energies appearing in Eq. (3). A single deposition rate $\rho = 0.25$ ML/s has been used. The two exchange energies for cation $E_{\text{In/Ga}}^i$ are taken as the values proposed in previous papers:[24] $E_{\text{In/Ga}}^{b \rightarrow s} = 1.8$ eV and $E_{\text{In/Ga}}^{s \rightarrow b} = 2.0$ eV; $\Delta_{\text{In/Ga}} > 0$ implies In segregation. No values for $E_{\text{Sb/As}}^{b \rightarrow s}$ and $E_{\text{Sb/As}}^{s \rightarrow b}$ have been previously reported in the literature, so we fix them by fitting the growth model to the experimental Sb concentration profiles measured via cross-sectional scanning tunneling microscopy (STM).[7] The profiles were measured for two different samples: SL1, $(\text{GaIn}_{0.25}\text{Sb})_{6.5}/(\text{InAs})_{15.5}$, at a growth temperature 380 °C, and SL2, $(\text{GaIn}_{0.23}\text{Sb})_6/(\text{InAs})_{14}$, at a growth temperature 440 °C.
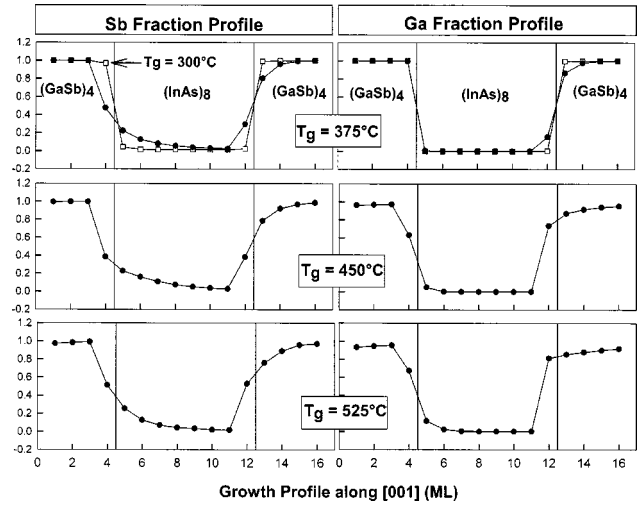

FIG. 4. Segregated profiles obtained for nominally $(\text{InAs})_8/(\text{GaSb})_8$ super-lattices as a function of the growth temperature. Deposition rate is 0.25 ML/s.

The fit to the experimental profiles gives $E_{\text{Sb/As}}^{b \rightarrow s} = 1.68$ eV and $E_{\text{Sb/As}}^{s \rightarrow b} = 1.75$ eV. The fit has been described in detail in Ref. 25. The fit is excellent except for the very first monolayer, where we neglected any surface reconstruction. Our determined $\Delta_{\text{Sb/As}} > 0$ shows that Sb segregates into the InAs layer, as observed.[7] $E_{\text{Sb/As}}^{b \rightarrow s}$ and $E_{\text{Sb/As}}^{s \rightarrow b}$ are both smaller than $E_{\text{In/Ga}}^{b \rightarrow s}$ and $E_{\text{In/Ga}}^{s \rightarrow b}$, so at very low growth temperatures (<375 °C) only anion segregation will be important, whereas appreciable In segregation is expected at higher temperatures (>375 °C).

Having obtained the segregation parameters for the InAs/GaSb system, we next model the atomistic structure of the superlattices used for optical studies. We consider superlattices lattice matched to a GaSb substrate. While we have modeled the profile along the [001] growth direction no experimental information is available on the atomistic arrangement in the perpendicular substrate (001) plane. We thus assume random arrangements in these planes, consistent with the planar composition profile dictated by the growth model. To achieve this we use a surface unit cell containing 16 atoms in the (001) plane, which are distributed randomly. Once we determine the superlattice configuration consistent with the solution of the growth model at a given growth temperature T_g, we permit local atomic displacements by VFF approach.[20]

Figure 4 shows the anion and cation segregation profiles obtained for a $(\text{InAs})_8/(\text{GaSb})_8$ superlattice at different growth temperatures and using a deposition rate $\rho = 0.25$ ML/s. We can see from the Ga profile the progressive shift with T_g of the first Ga plane backward inside the InAs well at the inverted (GaSb-on-InAs) interface. This is due to the large difference $\Delta_{\text{In/Ga}}$. At the higher T_g, when the first Ga atomic layer is deposited onto the InAs surface, almost all the Ga atoms exchange their position with the In atoms in the layer below. These In atoms are progressively pushed forward until, ultimately they reach the next interface, the InAs-on-GaSb normal interface. A similar substitution of the last
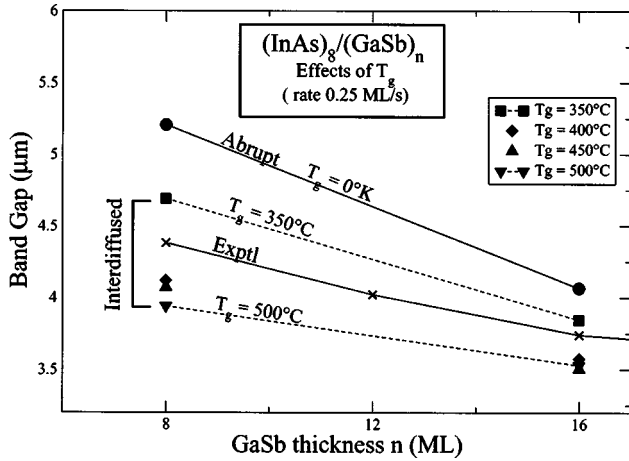
FIG. 5. Blueshift of the band gap of $(InAs)_8/(GaSb)_8$ and $(InAs)_8/(GaSb)_{16}$ superlattices with increasing growth temperature T_g. The experimental band gaps deduced from the absorbance data of Kaspi et al. (Ref. 28), are given for comparison (crosses).

As plane of InAs with an progressively (with T_g) higher fraction of Sb atoms occurs at the same inverted interface. The mechanism here is different and it is due, instead, to As segregation which is made possible by the small value of $\Delta_{Sb/As}$. Thus, we can see that the combination of a large $\Delta_{In/Ga}$ for cation segregation and a small $\Delta_{Sb/As}$ for anion segregation causes the narrowing of the InAs electron well with increasing T_g. The calculated profiles closely agree with the STM images of the anion sublattice of Ref. 7, where it is seen that the normal interface is rougher and broader than the inverted interface. This is due to the anion intermixing which is much larger at the normal interfaces than at the inverted interfaces (where only the one monolayer shift of a GaSb layer into InAs takes place). These results are in good agreement with many experimental findings.[7,26,27]

E. Blueshift of the band gap of segregated InAs/GaSb superlattices versus ideal structures

Through the kinetic model of MBE growth we can obtain realistic composition profiles for the segregated superlattices along the growth direction. Next, we need to build the entire superlattice atomistic structure. No experimental information is available on the atomistic arrangement in the planes perpendicular to the growth direction. We, thus, assume random arrangements in these planes, consistent with the planar composition profile dictated by the growth model. Once we have determined the superlattice configuration relative to a given growth temperature T_g and deposition rate ρ we allow local atomic displacements minimizing the strain energy of the structure using a valence force field approach.[20]

We apply our atomistic empirical pseudopotential technique to assess the effects on the band structure of the segregation at different growth temperatures, T_g. Figure 5 shows the trend of the band gaps as a function of the superlattice growth temperature T_g for the $(InAs)_8/(GaSb)_8$ and the $(InAs)_8/(GaSb)_{16}$ superlattices. In Fig. 5 we report also the experimental band gaps as deduced from the absorbance
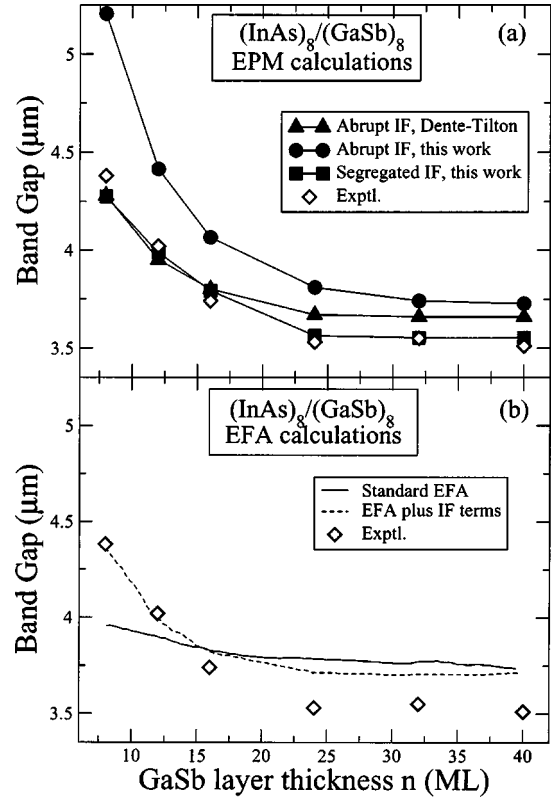

FIG. 6. Comparison of the experimental data (empty diamonds) for the $(InAs)_8/(GaSb)_n$ band gaps with the values given by (a) the EPM of Dente et al. (solid triangles) and by our EPM for superlattices with abrupt (solid circles) and segregated (solid squares) interfaces and (b) by the standard EFA method (continuous curve) and by EFA plus interface terms (see Ref. 30) (dashed curve). The lines are guidelines for the eye.

data of Kaspi et al.[28] for the $(InAs)_8/(GaSb)_n$ superlattices with $n = 8$, 12, 16. We see that abrupt SLs produce significantly (up to 50 meV) smaller gaps than SLs with intermixed interfaces. Since interfacial mixing is a fact (X-STM), one must compute band gaps of nonideal interfaces. The blueshift of the band gaps with increasing sample growth temperature is in agreement with the trend observed recently by Yang et al.[8] The band gap wavelength decrease (blueshift) with T_g is larger for the $(InAs)_8/(GaSb)_8$ superlattice than for the $(InAs)_8/(GaSb)_{16}$ superlattice, and also the difference between the band gap wavelength of the ideal abrupt geometry and that of the segregated ones is larger for the $(InAs)_8/(GaSb)_8$ superlattice.

F. Blueshift of $(InAs)_8/(GaSb)_n$ superlattices versus GaSb thickness n

In Fig. 6 we compare our results for the band gaps of the $(InAs)_8/(GaSb)_n$ superlattices with abrupt and segregated interfaces with those predicted by other calculations. We note the following features:

(i) Assuming artificially abrupt interfaces, our atomistic empirical pseudopotential approach predicts much smaller band gaps than the Dente and Tilton's empirical pseudopotential approach.[22] Since the pseudopotentials are similar for the bulk solids, the main reason for the differences has to

stem from the different treatment of the interfacial regions. The Dente–Tilton approach describes the interface through a step function, which leads to a very abrupt potential change at the interface between the InAs potential and the GaSb potential.[29] In our approach, instead, the change is more gradual and the interfacial Ga–As and In–Sb bonds are correctly described.

(ii) While the Dente and Tilton approach fit the experimental gap versus thickness curve for *abrupt* superlattices, our atomistic pseudopotential fits the experiment well only for segregated superlattices. Since interfacial intermixing is an experimental fact, the agreement of the theory for intermixed SLs with the experiment is gratifying.

(iii) The envelope function calculation by Lau *et al.*[30] with interfacial terms added to optimize the agreement with the experiment fits the experiment well for $n \lesssim 16$. At larger n approaches our result for the band gaps of abrupt interfaces. However, this approach is also not predictive (i.e., one parameter was adjusted to obtain agreement with the same gaps versus GaSb thickness experimental data).

(iv) The predicted blueshift of the band gap with respect to GaSb thickness n is only 47 meV for the EFA approach and 49 meV for the pseudopotential approach of Dente *et al.*, considerably smaller than the experimental value, 70 meV. Our predicted blueshifts for the same superlattices are 64 meV for segregated interfaces, and 95 meV for abrupt interfaces.

IV. CONCLUSIONS

We have presented in this article a fully atomistic approach to band structure calculations based on an empirical pesudopotential method and integrating new features such as (i) a consistent treatment of the local strain around the atoms and in the structure; (ii) an appropriate description of all the bonds present in the quaternary InAs/GaSb system, not only the bulk Ga–Sb and In–As bonds but also the *interface specific* bonds Ga–As and In–Sb; and (iii) an improved transferability scheme where the first neighbor environment of each atom is taken into account. We have shown that our scheme is capable, when combined with a kinetic model of MBE growth, of successfully describing interfacial segregation and intermixing effects in InAs/GaSb superlattices, since it possesses the necessary sensitivity to the microscopic atomic configurations in the system. Our scheme reproduces correctly trends of the fundamental gap with: (a) interfacial bond composition; (b) alloying; (c) interfacial segregation; and (d) superlattice period, which have been observed experimentally.

ACKNOWLEDGMENTS

[1] J. R. Meyer, L. J. Olafsen, E. H. Aifer, W. W. Bewley, C. L. Felix, I. Vurgaftman, M. J. Yang, L. Goldberg, D. Zhang, C. H. Lin, S. S. Pei, and D. H. Chow, IEE Proc.: Optoelectron. **145**, 275 (1998).

[2] S. H. Kwok, H. T. Grahn, K. Ploog, and R. Merlin, Phys. Rev. Lett. **69**, 973 (1993).

[3] R. Magri and A. Zunger, Phys. Rev. B **62**, 10364 (2000).

[4] O. Krebs and P. Voisin, Phys. Rev. Lett. **77**, 1829 (1996); O. Krebs, D. Rondi, J. L. Gentner, L. Goldstein, and P. Voisin, *ibid.* **80**, 5770 (1998).

[5] P. Pfeffer, Phys. Rev. B **59**, 15902 (1999).

[6] D. Gershoni, C. H. Henry, and G. A. Baraff, IEEE J. Quantum Electron. **29**, 2433 (1993).

[7] J. Steinshnider, M. Weimer, R. Kaspi, and G. W. Turner, Phys. Rev. Lett. **85**, 2953 (2000); J. Steinshnider, J. Harper, M. Weimer, C. H. Lin, S. S. Pei, and D. H. Chow, *ibid.* **85**, 4562 (2000).

[8] M. J. Yang, W. J. Moore, B. R. Bennet, and B. V. Shanabrook, Electron. Lett. **34**, 270 (1998); M. J. Yang, W. J. Moore, B. R. Bennet, B. V. Shanabrook, J. O. Cross, W. W. Bewley, C. L. Felix, I. Vurgaftman, and J. R. Meyer, J. Appl. Phys. **86**, 1796 (1999).

[9] I. Vurgaftman, J. R. Meyer, and L. R. Ram-Mohan, J. Appl. Phys. **89**, 5815 (2001).

[10] B. R. Bennett, B. V. Shanabrook, R. J. Wagner, J. L. Davis, J. R. Waterman, and M. E. Twigg, Solid-State Electron. **37**, 733 (1994).

[11] A. Zunger, Phys. Status Solidi A **190**, 467 (2002).

[12] J. P. Perdew and A. Zunger, Phys. Rev. B **23**, 5048 (1981).

[13] R. Magri, L. L. Wang, A. Zunger, I. Vurgaftman, and J. R. Meyer, Phys. Rev. B **61**, 10235 (2000).

[14] M. Cohen and V. Heine, in *Solid State Physics*, edited by H. Ehrenreich, F. Seitz, and D. Turnbull (Academic, New York, 1970), Vol. 24, p. 64.

[15] *Semiconductors: Group IV and III–V Compounds*, edited by O. Madelung, Landolt-Börnstein, New Series, Group III, Vol. 17 (Springer, Berlin, 1982); *Semiconductors: Intrinsic Properties of Group IV Elements and III–V, II–VI, and I–VII Compounds*, edited by O. Madelung, Landolt-Börnstein, New Series, Group III, Vol. 22 (Springer, Berlin, 1987).

[16] S.-H. Wei and A. Zunger, Appl. Phys. Lett. **72**, 2011 (1998).

[17] R. Magri and A. Zunger, Phys. Rev. B **65**, 165302 (2002).

[18] J. A. Van Vechten and T. K. Bergstresser, Phys. Rev. B **1**, 3351 (1970).

[19] D. Olego, M. Cardona, and H. Muller, Phys. Rev. B **22**, 894 (1980).

[20] P. Keating, Phys. Rev. **145**, 637 (1966).

[21] L. W. Wang and A. Zunger, J. Chem. Phys. **100**, 2394 (1994).

[22] G. C. Dente and M. L. Tilton, J. Appl. Phys. **86**, 1420 (1999); Phys. Rev. B **66**, 165307 (2002).

[23] M. J. Yang, C. H. Yang, B. R. Bennett, and B. V. Shanabrook, Phys. Rev. Lett. **78**, 4613 (1997).

[24] O. Dehaese, X. Wallart, and F. Mollot, Appl. Phys. Lett. **66**, 52 (1995).

[25] R. Magri and A. Zunger, Phys. Rev. B **64**, 081305 (2001).

[26] R. M. Feenstra, D. A. Collins, D. Z. Y. Ting, M. W. Wang, and T. C. McGill, Phys. Rev. Lett. **72**, 2749 (1994).

[27] M. E. Twigg, B. R. Bennett, P. M. Thibado, B. V. Shanabrook, and L. J. Whitman, Philos. Mag. A **7**, 7 (1998).

[28] R. Kaspi, C. Moeller, A. Ongstad, M. L. Tilton, D. Gianardi, G. Dente, and P. Gopaladasu, Appl. Phys. Lett. **76**, 409 (2000); A. P. Ongstad, R. Kaspi, C. E. Moeller, M. L. Tilton, D. M. Gianardi, J. R. Chavez, and G. C. Dente, J. Appl. Phys. **89**, 2185 (2001).

[29] G. C. Dente and M. L. Tilton, Phys. Rev. B **66**, 165307 (2002).

[30] W. H. Lau and M. E. Flatté, Appl. Phys. Lett. **80**, 1683 (2002).